JACS
JOURNAL OF THE AMERICAN CHEMICAL SOCIETY
Article
pubs.acs.org/JACS

Atomic Mechanism of Dynamic Electrochemical Lithiation Processes of MoS_2 Nanosheets

Lifen Wang, Zhi Xu, Wenlong Wang, and Xuedong Bai*

Beijing National Laboratory for Condensed Matter Physics and Institute of Physics, Chinese Academy of Sciences, Beijing 100190, China

Supporting Information

ABSTRACT: Layered molybdenum disulfide (MoS_2) has been studied for decades for its diversity of structure and properties, where the structural dynamic evolution during lithium intercalation is an important but still indistinct, controversial topic. Here the electrochemical dynamic process of MoS_2 nanosheets upon lithium intercalation has been systematically investigated by *in situ* high-resolution transmission electron microscopy. The results indicate that the lithiated MoS_2 undergoes a trigonal prismatic (2H)-octahedral (1T) phase transition with a lithium ion occupying the interlayer S−S tetrahedron site in the 1T-$LiMoS_2$. A pseudoperiodic structural modulation composed of polytype superlattices is also revealed as a consequence of the electron−lattice interaction. Furthermore, the shear mechanism of the 2H-1T phase transition has been confirmed by probing the dynamic phase boundary movement. The *in situ* real-time characterization at atomic scale provides a great leap forward in the fundamental understanding of the lithium ion storage mechanism in MoS_2, which should be also of help for other transition metal dichalcogenides.

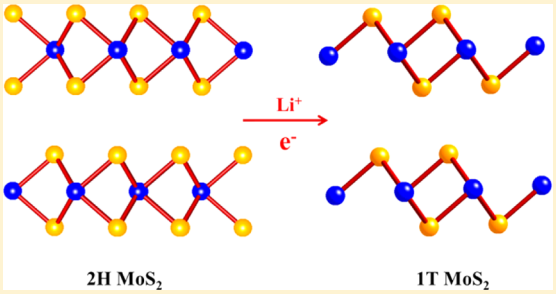

INTRODUCTION

Layered molybdenum disulfide (MoS_2) shows a unique combination of valuable structural, electronic, optical, mechanical, chemical, and thermal properties that have been studied for decades.[1] The inexpensiveness and availability have offered the uses for lubricant,[2] optoelectronic,[3] catalytic,[4] and clean energy storage applications.[5] Its lamellar structure and properties are also beneficial for high power applications such as solid state batteries and supercapacitors.[6] The weak van der Waals interaction between the MoS_2 layers allows alkali ions to intercalate without a significant volume expansion, which enables MoS_2 to be an alternative as an electrode material for high capacity lithium ion batteries.[7,8] It has been known that MoS_2 has a good cycling behavior at ∼2 V of discharging voltage, even at low temperature.[9] Research on the lithium ion reaction mechanism of MoS_2 is a significant field, both in fundamental studies and practical application.

MoS_2 by its nature is a semiconductor with trigonal (2H) structure, where the S atoms locate in the lattice position of a hexagonal close-packed structure. Planes of Mo atoms are sandwiched between two atomic layers of S, such that each Mo is coordinated to six S atoms in a trigonal prismatic geometry (2H). Another MoS_2 polytype based on tetragonal symmetry is the octahedral phase (1T) with one MoS_2 layer per repeat unit (schematic coordination shown in Supplemental Figure S1). A structural transformation of 2H-1T due to lithium ion intercalation has been suggested,[10−12] and the corresponding electronic structure change from semiconducting to metallic has been observed by photoluminescence measurement.[13] However, the conventional *ex situ* studies introduced a complicated post-treatment process, where multiple unexpected factors were involved and made it too complicated to clarify the structure transformation. The accompanying co-intercalation of solvent molecules with lithium ions, for example, hindered the investigation of the accurate mechanism. Based on the "exfoliated and restacked" Li_xMoS_2 system, the precise structural information on the new phase such as the lithium ion intercalation site has not coincided within the previous literature,[14−20] let alone the transition mechanism.

Here we examined the complete lithium intercalation process in lamellar MoS_2 nanosheets via an *in situ* transmission electron microscopy (TEM) approach, realizing a real-time imaging characterization of the electrochemical process at the atomic level that greatly advances the understanding of the phase transition mechanism and the correlation between structural and electrochemical properties in MoS_2. The new results, for the first time, thoroughly demonstrate the existence of a phase transition from pristine 2H-MoS_2 to 1T-$LiMoS_2$, which is composed of polytype superlattices with a lithium ion occupying the interlayer S−S tetrahedron site. Moreover, $LiMoS_2$/dislocation-decorated buffer region/pristine-MoS_2 was recorded simultaneously at the phase boundary, revealing a shear mechanism for the 2H-1T phase transition. Although with a high content of intercalated lithium ions a conversion reaction from 1T-$LiMoS_2$ to Mo/Li_2S followed, a volume

Received: February 20, 2014
Published: April 11, 2014

dx.doi.org/10.1021/ja501686w | J. Am. Chem. Soc. 2014, 136, 6693−6697

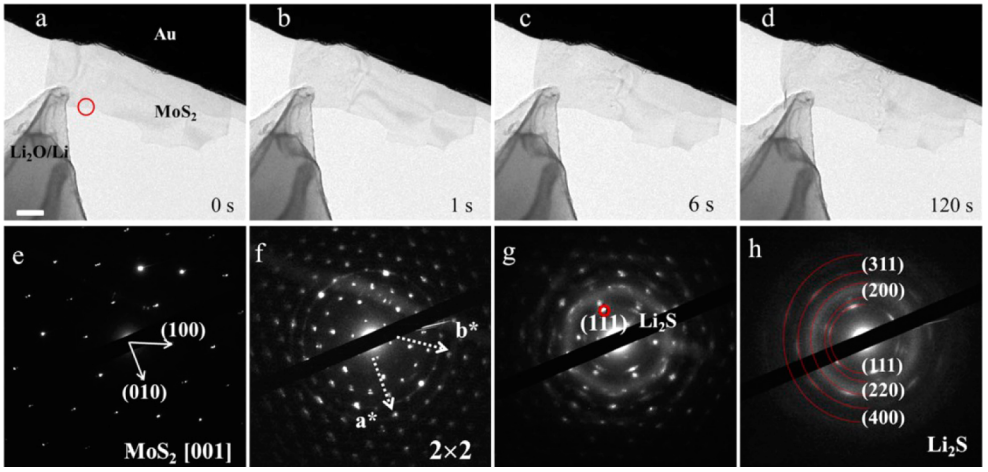

Figure 1. *In situ* electrochemical reaction of lamellar MoS_2 nanosheets with lithium. (a–d) Time-lapse TEM image records of morphological evolution of a MoS_2 nanosheet during the first lithium ion reaction process with reaction duration of 0, 1, 6, and 120 s, respectively. Scale bar, 0.2 μm. (e–h) In situ electron diffraction patterns (EDPs) of the same area marked by the red circle in panel a along the [001] zone-axis direction during the reaction process. Pristine EDP is shown in panel e with 0 s of reaction time; one set of superstructure spots appears in panel f after 1 s of lithiation. With longer lithiation time (6 s), diffraction spots of Li_2S show up in panel g. After 120 s, the lithiated MoS_2 is finally converted to amorphous Li_2S in panel h.

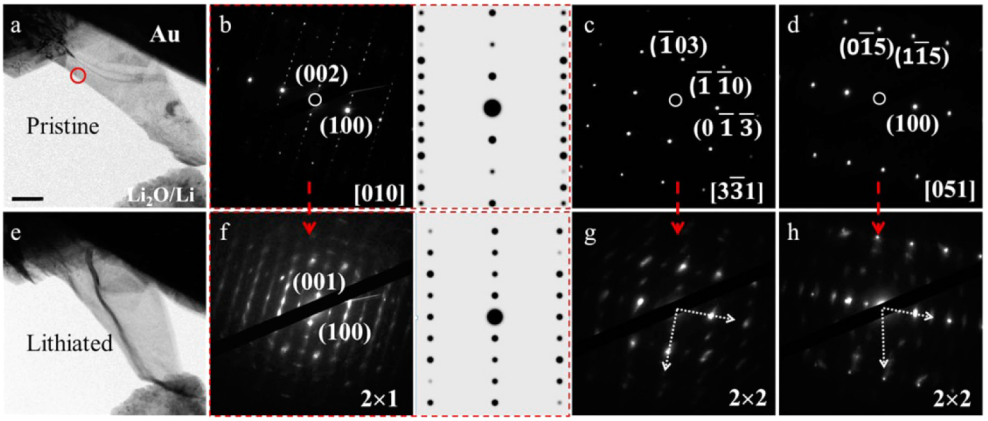

Figure 2. Phase transition probed by *in situ* EDPs. (a,e) TEM images of a MoS_2 nanosheet taken before and after the lithium ion intercalation. The red circle indicates the selected region on which the EDPs are taken and analyzed. Scale bar, 0.2 μm. (b–d) EDPs taken before the lithium ion intercalation along the [010], [3$\bar{3}$1], and [051] zone-axes, respectively. The simulant EDP of the pristine 2H-MoS_2 along the [010] zone-axis is also shown in panel b. (f–h) EDPs taken after the lithium ion intercalation along the [010], [3$\bar{3}$1], and [051] zone-axes, respectively. The simulant EDP of the crystalline 1T-MoS_2 along the [010] zone-axis is provided in panel f, for comparison purpose.

change of no more than 35% was introduced to the MoS_2 with stable lamellar structure maintained during the lithiation process.

RESULTS AND DISCUSSION

Before the *in situ* measurement, discharge/charge studies of MoS_2 powder were first conducted in the coin-type cell. Two apparent plateaus are observed in the first discharge process, indicating that the MoS_2 electrode undergoes two structural transformations during the first lithiation process[1,10,11] (see the details in the Supporting Information). To directly capture the dynamic structural changes, open Li/Li_2O/MoS_2 lithium cells were built and characterized via real-time *in situ* high resolution transmission electron microscopy (HRTEM) imaging, electron diffraction (ED), and electron energy-loss spectroscopy (EELS). The lamellar MoS_2 electrodes were prepared by peeling off a very thin sheet from the single crystal MoS_2 bulk and further incorporated into a homemade double-tilt TEM specimen holder.[21,22] A constant current of 5 nA or 500 pA between 0 and 5 V was applied across the cell to lithiate the MoS_2 nanosheets. Recently, it was reported that the 1T phase can be introduced in the 2H-MoS_2 single layer by using a high dose incident electron beam during heating of the MoS_2 single layers.[23] In our experiment, to exclude the influence of the electron beam, the reaction was recorded at subsecond temporal resolution with a small dose of electron beam at room temperature.

Time-lapse electron diffraction patterns (EDPs) of the MoS_2 taken in the near-surface region clearly show a remarkable feature that the lithiation of the pristine MoS_2 induces structural transformations (Figure 1). Upon lithiation as recorded in Figure 1a–d, a reaction front is introduced, which then propagates extremely fast and sweeps across the MoS_2 sheet within a few seconds. Figure 1e–h presents the EDPs acquired from the same region marked by a red circle in Figure 1a after a reaction duration of 0, 1, 6, and 120 s, respectively. The [001] zone-axis EDP from the pristine 2H-MoS_2 (Figure 1e) shows one set of 6-fold symmetry diffraction

dx.doi.org/10.1021/ja501686w | J. Am. Chem. Soc. 2014, 136, 6693–6697

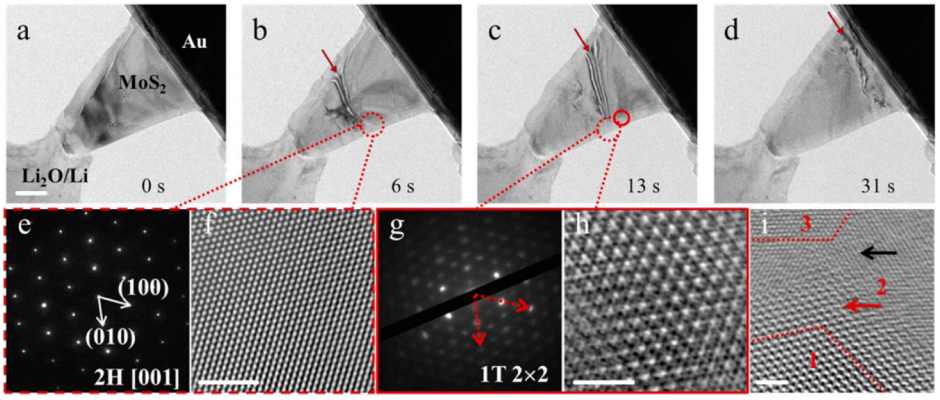

Figure 3. Phase boundary in 2H-1T phase transition. (a–d) Sequential TEM images of the morphological evolution of a MoS_2 nanosheet during the first lithiation process. Arrows show the wavy surface in the reaction front. Scale bar, 0.2 μm. (e,f) EDP and TEM image of an area ahead of the reaction front. Scale bar, 2 nm. (g,h) Corresponding records from the same area after the lithium ion intercalation. Scale bar, 2 nm. (i) HRTEM image of the 2H/1T phase boundary. Three regions are determined by three different feathers: region 1 showing the lithium intercalated phase with a superlattice, region 3 indicating the unreacted pristine phase, and region 2 with dislocations between region 1 and region 3. The red arrow points out the wavy-distorted structure near the superstructure; the black arrow highlights the slip dislocations close to the pristine structure. Scale bar, 2 nm.

spots. After 1 s of lithiation, surprisingly, the commensurate superstructure reflections appear along a* (100) and b* (010) directions with a 2-fold periodicity (Figure 1f), and this pattern arising from the superstructure can be characterized by two primary modulation vectors (1/2) a* and (1/2) b* (a* = b*). As given by ED results, Li_xMoS_2 displays a 2×2 superstructure in the a–b plane. The structure transformation from the pristine 2H form to the 2×2 superstructure is believed to be related to phase transition at the first discharge plateau around 1.1 V in Supplemental Figure S2. With longer lithiation time (6 s), another set of diffraction patterns is superimposed (Figure 1g). The newly appeared diffraction spots indicate the formation of Li_2S, corresponding to the second discharge plateau (Supplemental Figure S2). Finally, the fully lithiated MoS_2 is converted to an amorphous Li_2S matrix without any superstructure remaining (Figure 1h). This structural evolution can be described with the following types of structures: a 2×2 superstructure of Li_xMoS_2, a 2×2 superstructure dispersing in amorphous Li_2S matrices, and an amorphous Li_2S structure in the fully lithiated phase, which coincides with the *ex situ* result.[24] Note that such regularity is a typical feature in our experiment. Another example is shown in Supplemental Figure S3.

To understand the phase transition of MoS_2 during lithium intercalation comprehensively, the degree of lithiation was monitored and tuned by controlling the applied current. Therefore, the modulated MoS_2 structure by lithium ion intercalation can be kept at the desired intercalation stage during the first lithiation process. The intermediate stage of lithiation process is puzzling but so appealing. Here we controlled the lithiation process to stop at the stage of a 2×2 superstructure of Li_xMoS_2, corresponding to that shown in Figure 1f. Meanwhile, multiply zone-axes EDPs can also be recorded. Figure 2 shows a series of selected area EDPs of the MoS_2 taken before (Figure 2b–d) and after (Figure 2f–h) the intercalation reaction along zone-axes of [010], [$3\bar{3}1$], and [051], respectively (The real-time movie is shown in Supplemental Movie 1). The pristine MoS_2 has an EDP with sharp Bragg spots alternating with dim ones in the (001) orientation under observation along the [010] zone-axis direction, which is in accordance with the corresponding EDP simulation of 2H-MoS_2 in a rigorous way (Figure 2b). After the lithium ion intercalation, superstructure reflection appears along the symmetry (100) direction with a 2-fold periodicity. More remarkably, Bragg spots along the (001) orientation become equally sharp and intense, suggesting a notable alternation in crystal symmetry; this pattern is attributed to the 1T symmetry, which is strongly supported by the EDP simulation of the crystalline 1T-MoS_2 along the [010] zone-axis (Figure 2f). Such symmetry change revealed by diffraction comparison testified to the phase transition from crystalline 2H-MoS_2 to structure modulated 1T-Li_xMoS_2 by lithium ion intercalation.

Moreover, which site the Li ion occupies in the new 1T-Li_xMoS_2 phase is still an interesting and open topic. 1T-MoS_2 host lattices have tetrahedral and octahedral cavities between sulfur atoms for the Li atom in the van der Waals gap.[25] The Li ion concentration and occupation play a dominant role in the unit cell parameter of the Li_xMoS_2. Here, according to the multiply zone-axes EDP results of the MoS_2 nanosheet before and after the intercalation reaction, the unit cell parameter evolution of the 1T-Li_xMoS_2 from the pristine 2H-MoS_2 can be precisely ascertained. The lattice along *a*-axis expands subtly, while the value in the *c*-axis direction expands to 14 from 12.3 Å. The crystal geometry and formation energies for a large set of 1T-Li_xMoS_2 intercalates have been investigated systematically using the density functional theory approach.[25] By combining the experimental data and the theoretical calculations, the lithium ion is considered to reside in the interlayer S–S tetrahedron site in the 1T-$Li_{1.0}MoS_2$ as the most favorable intercalation sites.

In addition to 2H-1T phase transition, Li ion intercalation also gives rise to another structure modulation. The 2-fold periodic modulation is observed in Figure 2f–h, which is consistent with the superstructure in the a–b plane as shown in Figure 1 (see other data in Supplemental Figure S4). Those EDPs can be well apprehended by projecting the basic 1T-$LiMoS_2$ structure with 2-fold periodicity modulation in the corresponding directions. With in-depth analysis above, the structural property of the new phase produced by lithium ion intercalated MoS_2 is ascertained with comprehensive details.

dx.doi.org/10.1021/ja501686w | *J. Am. Chem. Soc.* 2014, 136, 6693–6697

Distinct contrast and morphological transformation of MoS_2 nanosheet are always accompanied by Li ions intercalation in our experiment. Figure 3 shows one representative time-lapse structural changes of the layered 2H-MoS_2 during the first discharge (see Supplemental Movie 2). Along with the reaction, a wavy front pointed out by arrows in Figure 3b–d shows up and propagates along the lithium ion intercalation direction. The wavy surface in the reaction front can be attributed to a combination of multiple factors, including a sliding motion of slabs with respect to each other, changing of sites of the Mo atoms associated with Fermi surface nesting, and the John-Teller effect.[26−33] Given that Mo and S planes have different relative coordination in the 2H and 1T phases, the wavy structure indicates the phase transition involves a slipping of slabs in the MoS_2 crystal. A near surface area marked by the dotted red circle was chosen on which to perform structure comparison before and after the wavy front passes by. The EDP and HRTEM images shown in Figure 3e and f show the pristine 2H structure clearly. The structure information shown in Figure 3g and h was acquired immediately after the wavy front passed by, suggesting the lithium ion intercalated phase. This phenomenon provides a hint that the wavy front is actually the lithium ion intercalation front. Consequently, we have the capability to determine the dynamic interfacial structure, which is essential for understanding the kinetics of the lithium ions transport, the movement of the phase boundary, and the structure transition. As clearly concluded from the HRTEM image of the boundary area in Figure 3i, the reaction front is divided into three regions. Region 1 is the lithiated part with a superlattice, and the unreacted part is region 3, displaying a pristine structure. A relaxation buffer area named region 2 exists between the two other regions and is full of dislocations. This kind of relaxation could result from diffusion-limited kinetic effects.[34] In region 2, two different features are found: a wavy periodic structure near the lithiated side and a distortion area full of slip dislocations next to the unreacted part. Existence of the slip dislocations is also confirmed by the elongation of the diffraction spots (Figure 1f). The ∼10 nm wide dislocation zone in the buffer region indicates the existence of the strain introduced by the shear transformation of slabs. The underlying force is the lithium ion intercalation, which triggers the sliding of slabs in MoS_2 and gradually produces the 1T-$LiMoS_2$.

The 2×2 superstructure in the a–b plane is a typical feature of the intercalated samples in our experiment. A further understanding of the superlattice is gleaned from studying the microdomains shown in Figure 4, demonstrating a simultaneous formation of polytype sublattices. Figure 4a shows the HRTEM image of the intercalated MoS_2, and the Fast Fourier Transform (FFT) of the image (inset) indicates a 2×2 superstructure. Three areas were selected to explore the microdomains as shown in Figure 4b–d. Detailed investigation of these microdomains reveal that the 2×2 superstructure in Figure 4a is composed of a variety of sublattices, including 2×1 (Figure 4b), $\sqrt{3}$×1 (Figure 4c), and 2×2 (Figure 4d). These subsuperlattices are in good agreement with charge-density wave (CDW) theory, which has predicted the d-electron count dependence of the structural modulations of transition metal dichalcogenides (TMDCs) layers on the basis of their hidden one-dimensional Fermi surfaces.[35] The electronic instabilities of low-dimensional metals lead to their metal–metal-bonded clusters, showing an electron–lattice interaction. Here, as found in our *in situ* experiments, the sublattices include zigzag-chain

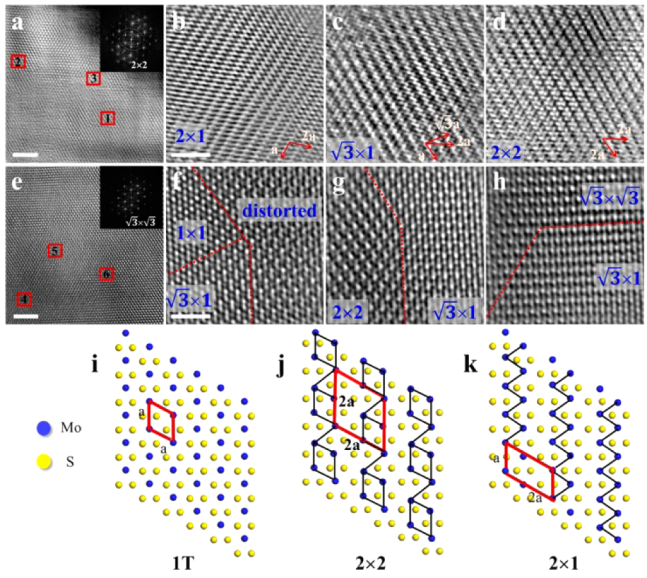

Figure 4. Subsuperlattices in lithium intercalated MoS_2. (a) HRTEM image of lithium ion intercalated MoS_2 taken along the [001] zone-axis direction. The FFT data (inset) show a 2×2 superstructure. Scale bar, 5 nm. (b–d) HRTEM images of microdomain structures derived from different areas in panel a marked by red squares 1, 2, and 3, respectively, showing three different subsuperlattices. Scale bar, 2 nm. (e) HRTEM image of another MoS_2 nanosheet obtained by smaller lithiation current. The FFT data (inset) shows a superstructure. Scale bar, 5 nm. (f–h) HRTEM images of complex subsuperlattices taken from different regions marked by red squares 4, 5, and 6, respectively. Scale bar, 2 nm. (i) Schematic of the atom structures in the a–b plane of the natural 1T structure. (j,k) Schematics illustrating the atom structures in the a–b plane of 2×1 and 2×2 structures formed by different Mo–Mo clusters, respectively.

clustering of Mo atoms in the d^2 system forming the zigzag superstructure (Figure 4b), ribbon-chain clustering of Mo atoms in the $d^{3/4}$ system forming the ribbon-chain superstructure (Figure 4c), and diamond-chain clustering of Mo atoms in the d^3 system forming the diamond-chain superstructure (Figure 4d). Figure 4e shows the TEM image of another sample that was obtained by the lithiation of MoS_2 nanosheets under smaller constant current (50 pA). The inset shows the FFT data, revealing that it has a superstructure. In a similar way, this structure consists of microdomains including 1×1, $\sqrt{3}$×$\sqrt{3}$, $\sqrt{3}$×1, and 2×2 subsuperlattices correspondingly shown in Figure 4f–h. All these sublattices except 1×1 can be obtained from $\sqrt{3}$×1 superlattice by "twinning" or "triplicating" itself. To clarify the superstructure modulation, Figure 4i–k shows the schematics illustrating the atom structures in the a–b plane of the natural 1T, 2×1, and 2×2 structures, respectively. Note that the superstructures in the 1T-$LiMoS_2$ are transient states,[36−38] which were found in our experiment to disappear and reduce to the 1T structure within a few days with exposure to air.

CONCLUSION

In conclusion, we have performed a systematical study of the structural properties of MoS_2 nanosheets during the lithiation process using an *in situ* electrochemical TEM technique. The results demonstrate the existence of a phase transition of 2H-MoS_2 to 1T-$LiMoS_2$ and structural modulation of clustering of the Mo atoms in the 1T-$LiMoS_2$. Furthermore, with the capability of characterizing the phase boundary, the shear

dx.doi.org/10.1021/ja501686w | J. Am. Chem. Soc. 2014, 136, 6693–6697

mechanism of the 2H-1T phase transition has been confirmed. Utilizing the *in situ* measurements, the electrochemical reaction in each stage has been thoroughly studied, which can also be correlated with the *ex situ* performance of MoS_2 coin-type cells. After the phase transition of 2H-MoS_2 to 1T-$LiMoS_2$, there follows a conversion reaction, i.e., 1T-$LiMoS_2$ + $xLi^+ \rightarrow Li_2S$ + Mo, during the lithiation of MoS_2. With our experiment, the structure corresponding to the electrochemical property of MoS_2 during lithiation can be clearly understood. Since lithium intercalation-based chemical exfoliation of layered TMDCs has been demonstrated as an effective method for preparing atomically thin layers in the liquid environment, the fundamental understanding of lithium ion intercalation behavior can allow for development in TMDCs-related energy devices and should enable a wide range of studies, such as TMDCs-based composition and optoelectronics.

EXPERIMENTAL SECTION

***In Situ* TEM Experiment.** Lamellar MoS_2 samples serving as working electrode were peeled off from an epitaxially grown single crystal by gold wires. In an argon-filled glovebox, metal lithium serving as counter electrode was scratched by electrochemically shaped tungsten tips. Both the gold wire with working electrode and the tungsten tip with metal lithium were loaded onto a homemade double-tilt TEM specimen holder inside the glovebox and sealed in a full argon-filled bag. The holder was transferred into the TEM column. The thin oxide layer on the surface of the metallic lithium served as the solid electrolyte. Once the Li_2O-covered Li electrode driven by a piezoceramic manipulator had contacted the free end of a selected sample, a constant current of 500 pA or 5 nA between 0 and 5 V was applied across the sample to lithiate the MoS_2. TEM characterization was performed using a JEOL 2010F transmission electron microscope operated at 200 keV at room temperature with a column vacuum ~1×10^{-7} Torr.

ASSOCIATED CONTENT

Supporting Information

Procedures and additional data. This material is available free of charge via the Internet at http://pubs.acs.org.

AUTHOR INFORMATION

Corresponding Author

xdbai@iphy.ac.cn

Notes

The authors declare no competing financial interest.

ACKNOWLEDGMENTS

We thank Liqiang Mai's group at Wuhan University of Technology for their ex situ comparison experiment of a MoS_2 coin-type cell. This work was supported by National 973 projects (Grant Nos. 2012CB933003 and 2013CB93200) from Ministry of Science and Technology, China.

REFERENCES

(1) Chhowalla, M.; Shin, H. S.; Eda, G.; Li, L. J.; Loh, K. P.; Zhang, H. *Nat. Chem.* **2013**, *5*, 263.
(2) Chhowalla, M.; Amaratunga, G. A. J. *Nature* **2000**, *407*, 164.
(3) Wang, Q. H.; Zadeh, K. K.; Kis, A.; Coleman, J. N.; Strano, M. S. *Nat. Nanotechnol.* **2012**, *7*, 699.
(4) Zong, X.; Yan, H.; Wu, G.; Ma, G.; Wen, F.; Wang, L.; Li, C. *J. Am. Chem. Soc.* **2008**, *130*, 7176.
(5) Julien, C.; Saikh, S. I.; Nazri, G. A. *Mater. Sci. Eng., B* **1992**, *15*, 73.
(6) Soon, J. M.; Loh, K. P. *Electrochem. Solid-State Lett.* **2007**, *10*, A250.
(7) Xiao, J.; Choi, D.; Cosimbescu, L.; Koech, P.; Liu, J.; Lemmon, J. P. *Chem. Mater.* **2010**, *22*, 4522.
(8) Hwang, H.; Kim, H.; Cho, J. *Nano Lett.* **2011**, *11*, 4826.
(9) Laman, F. C.; Matson, M. W.; Stiles, J. A. R. *J. Electrochem. Soc.* **1986**, *133*, 2441.
(10) Woollam, J. A.; Somoano, R. B. *Phys. Rev. B* **1976**, *13*, 3843.
(11) Benavente, E.; Ana, M. A. S.; Mendizàbal, F.; Gonzàlez, G. *Coord. Chem. Rev.* **2002**, *224*, 87.
(12) Somano, R. B.; Woollam, J. A. In *Intercalated Layered Materials*; D. Reidel: Dordrecht, 1979; p 307.
(13) Julien, C. *Mater. Res. Soc. Symp. Proc.* **1993**, *293*, 411.
(14) Heising, J.; Kanatzidis, M. G. *J. Am. Chem. Soc.* **1999**, *121*, 638.
(15) Heising, J.; Kanatzidis, M. G. *J. Am. Chem. Soc.* **1999**, *121*, 11720.
(16) Qin, X. R.; Yang, D.; Frindt, R. F.; Irwin, J. C. *Ultramicroscopy* **1992**, *42–44*, 630.
(17) Dungey, K. E.; Curtis, M. D.; Penner-Hahn, J. E. *Chem. Mater.* **1998**, *10*, 2152.
(18) Wypych, F.; Solenthaler, C.; Prins, R.; Weber, T. *J. Solid State Chem.* **1999**, *144*, 430.
(19) Wypych, F.; Weber, Th.; Prins, R. *Surf. Sci.* **1997**, *380*, L474.
(20) Miremadi, B. K.; Cowan, T.; Morrison, S. R. *J. Appl. Phys.* **1991**, *69*, 6373.
(21) Gao, P.; Kang, Z. C.; Fu, W. Y.; Wang, W. L.; Bai, X. D.; Wang, E. G. *J. Am. Chem. Soc.* **2010**, *132*, 4197.
(22) Wang, L. F.; Xu, Z.; Yang, S. Z.; Tian, X. Z.; Wei, J. K.; Wang, W. L.; Bai, X. D. *Sci. China Technol. Sci.* **2013**, *56*, 2630.
(23) Lin, Y. C.; Dumcenco, D. O.; Huang, Y. S.; Suenaga, K. *arXiv:13102363*, **2013**.
(24) Xiao, J.; Wang, X. J.; Yang, X. Q.; Xun, S. D.; Liu, G.; Koech, P. K.; Liu, J.; Lemmon, J. P. *Adv. Funct. Mater.* **2011**, *21*, 2840.
(25) Enyashin, A. N.; Seifert, G. *Comput. Theor. Chem.* **2012**, *999*, 13.
(26) Bronsema, K. D.; Boer, J. L.; Jellinek, F. Z. *Anorg. Allg. Chem.* **1986**, *540/541*, 15.
(27) Laundry, J.; Tendeloo, G.; Amelinckx, S. *Phys. Status Solidi A* **1974**, *26*, 585.
(28) Sandre, E.; Brec, R.; Rouxel, J. *J. Solid State Chem.* **1990**, *88*, 269.
(29) Yoffe, A. D. *Solid State Ionics* **1990**, *39*, 1.
(30) Joensen, P.; Crozier, E. D.; Alberding, N.; Frindt, R. F. *J. Phys. C: Solid State Phys.* **1987**, *20*, 4043.
(31) Sandoval, S. J.; Yang, D.; Frindt, R. F.; Irwin, J. C. *Phys. Rev. B* **1991**, *44*, 3955.
(32) Kertesz, M.; Hoffmann, R. *J. Am. Chem. Soc.* **1984**, *106*, 3453.
(33) Whangbo, M. H.; Canadell, E. *J. Am. Chem. Soc.* **1992**, *114*, 9587.
(34) Petsev, D. N.; Chen, K.; Gliko, O.; Vekilov, P. G. *Proc. Natl. Acad. Sci. U.S.A.* **2003**, *100*, 792.
(35) Burdett, J. K.; Hughbanks, T. *Inorg. Chem.* **1985**, *24*, 1741.
(36) Wypych, F.; Schollhorn, R. *J. Chem. Soc., Chem. Comm.* **1992**, *19*, 1386.
(37) Imanishi, N.; Toyoda, M.; Takeda, Y.; Yamamoto, O. *Solid State Ionics* **1992**, *58*, 333.
(38) Zubavichus, Y. V.; Slovokhotov, Y. L.; Schilling, P. J.; Tittsworth, R. C.; Golub, A. S.; Protzenko, G. A.; Novikov, Y. N. *Inorg. Chim. Acta* **1998**, *280*, 211.